Biosensors and Bioelectronics 79 (2016) 522–530

Contents lists available at ScienceDirect

Biosensors and Bioelectronics

journal homepage: www.elsevier.com/locate/bios

# Visual multiple recognition of protein biomarkers based on an array of aptamer modified gold nanoparticles in biocomputing to strip biosensor logic operations

Chunyan Qin, Ya Gao, Wei Wen, Xiuhua Zhang, Shengfu Wang *

*Hubei Collaborative Innovation Center for Advanced Organic Chemical Materials, Ministry of Education Key Laboratory for the Synthesis and Application of Organic Functional Molecules & College of Chemistry and Chemical Engineering, Hubei University, Wuhan 430062, PR China*

ARTICLE INFO

*Article history:*
Received 7 October 2015
Received in revised form
25 December 2015
Accepted 26 December 2015
Available online 29 December 2015

*Keywords:*
Aptamers
Gold nanoparticles
Protein
Logic gate
The strip biosensors array

ABSTRACT

We developed a strip biosensors array based on aptamer-modified gold nanoparticles as receptors and combined the protein-aptamer binding reaction with the streptavidin-biotin interaction as well as the sandwich format. We found that a series of protein receptors obtained a distinct response pattern to each target protein. Three proteins have been well distinguished with the naked eyes and a portable reader without mutual interference, accompanying with lower limit of detection and wider linear range. A complete set of four elementary logic gates (AND, OR, INH, and NAND) and eight combinative logic gates (AND–OR; AND–INH; OR–INH; INH–NAND; AND–OR–INH; AND–INH–NAND; OR–INH–NAND; AND–OR–INH–NAND) are thoroughly realized using this array, which could eventually be applicable to the keypad-lock system with enhanced complexity in the near future. Moreover, this array shows excellent linear relationships, anti-interference capability, real human serum samples applicability, long-term storage stability and reproducibility. All indicate that this design has very good prospects for development.



## 1. Introduction

Biomolecules possess excellent properties as building blocks, such as naturally availability in quantities, good biocompatibility, structurally diversity, chirality, multiple possible coordination modes, and prices amenability (Pu et al., 2014; Angelos et al., 2009). In the case of biomolecular ligands, aptamers are one of the ideal bio-linkers, which are single-stranded DNA or RNA oligonucleotides selected from large combinatorial libraries by systematic evolution of ligands by exponential enrichment (SELEX) (Wilson and Szostak, 1999; Tuerk and Gold, 1990; Cox and Ellington, 2001; Berezovski, 2005). The so-called aptamers offer great flexibility in terms of structure variants to bind to a variety of targets with high affinity and specificity, and they are also promising candidates for bioanalytical applications and new computing systems (Famulok and Mayer, 2011; Liu et al., 2010). Moreover, when a single aptamer splits into two fragments, they usually can form associated sandwich-type complexes with their targets (Feng et al., 2015). So far, most examples to control protein activity using aptamer are based on the streptavidin (SA)-biotin interaction or use a limited number of protein-binding aptamers (Qin et al., 2015a,b). Herein we extend this concept of a split aptamer-based strip biosensors array by modifying with gold nanoparticles (AuNPs) for visual multiple recognition of proteins.

Their synthetic accessibility and highly predictable binding properties make aptamers ideal building blocks to construct molecular logical circuits (Janssen et al., 2015; Stojanovic et al., 2014), which are molecular-scale computers that perform Boolean operations to carry out binary computational functions (Seelig et al., 2006). Despite previous burgeoning developments, most of the molecular logic systems have the following disadvantages: (1) it is difficult to scale them up for assembling large networking systems owing to the interference between reactions in the same chemical system and the incompatibility of various chemical gates operating under different conditions (Silva and Uchiyama, 2007); (2) they usually employ a fluorescent signal as the output, which relies on advanced instruments for the readout (Uchiyama et al., 2004); and (3) they often lack the desired portability and require sophisticated synthesis processes, which adds to the complexity, cost, and overall assay time (Lin et al., 2012).

Therefore, it would be highly desirable to develop logic system that is simple in design, not limited to solution-based applications, and involves a reliable and convenient readout. Moreover, a series of independently working logic gates could be easily brought together to function as concatenated logic gates. So, we designed a strip biosensors array to be an ideal pattern to monitor logic

* Corresponding author.
*E-mail address:* wangsf@hubu.edu.cn (S. Wang).

http://dx.doi.org/10.1016/j.bios.2015.12.096
0956-5663/

operations. Upon binding to proteins, it will generate a direct and visible readout, which can be readily distinguished by the naked eye. This also offers a platform for applying to the "keypad lock" system duo to its output signals are dependent not only on the proper combination of inputs but also on the order in which these inputs are introduced. Moreover, this array shows excellent accuracy for detecting protein biomarkers, anti-interference capability, real human serum samples applicability, and long-term storage stability. All indicate that this design has very good prospects for development.

## 2. Materials and methods

### 2.1. Chemicals and materials

Hydrogen tetrachloroaurate (III) trihydrate ($HAuCl_4 \cdot 3H_2O$), trisodium citrate, sucrose, trehalose, Tween-20, TritonX-100, Tris (2-carboxyethyl) phosphine (TCEP), deoxyadenosine triphosphate (DATP), $Na_3PO_4 \cdot 12H_2O$, 30% $H_2O_2$, phosphate buffer saline (PBS, PH 7.4, 0.01 M), bovine serum albumin (BSA), carcinoembryonic antigen (CEA) from human fluids (Z95%, SDS-PAGE), human serum, thrombin (TB) from human plasma were purchased from Sigma-Aldrich (USA). Streptavidin (SA) were purchased from Promega (USA). Goat anti Rabbit IgG were purchased from Thermo Scientific. Nitrocellulose membrane (HFB18002) was purchased from Millipore (Billerica, MA). Polyester fiber (VL78, CH27), laminated cards (SM31-40), HM3030 dispenser, CTD300P programmable strip cutter, DT2032 portable strip reader were purchased from Shanghai Kinbio Tech. Co., Ltd. Shanghai, China. Transmission electron microscopic (TEM) images were obtained on FEI Tecnai G20 (America) with an accelerating voltage of 200 kV. Hairpin oligonucleotide (HO), single-stranded DNA (ssDNA) and mucin 1 protein (MUC1) were synthesized and purified by Sangon (Shanghai, China).

The aptamer sequences were as follows:

Thrombin hairpin oligonucleotide (TB-HO): 5′-Biotin-AGT CCG TGG TAG GGC AGG TTG GGG TGA CT-(CH2)6-SH-3′

Thrombin single-stranded DNA (TB-ssDNA): 5′-AGT CCG TGG TAG GGC AGG TTG GGG TGA CT-(CH2)6-SH-3′

Thrombin test DNA (TB-tDNA): 5′-Biotin-AGT CCG TGG TAG GGC AGG TTG GGG TGA CT-3′

Thrombin control DNA (TB-cDNA): 5′-Biotin-AG TCA CCC CAA CCT GCC CTA CCA CGG ACT-3′

Mucin 1 protein hairpin oligonucleotide (MUC1-HO): 5′-Biotin-G CAG TTG ATC CTT TGG ATA CCC TGG-(CH2)6 -SH-3′

Mucin 1 protein single-stranded DNA (MUC1-ssDNA): 5′-G CAG TTG ATC CTT TGG ATA CCC TGG-SH-3′

Mucin 1 protein test DNA (MUC1-tDNA): 5′-Biotin-G CAG TTG ATC CTT TGG ATA CCC TGG-3′

Mucin 1 protein control DNA (MUC1-cDNA): 5′-Biotin-CCA GGG TAT CCA AAG GAT CAA CTG C-3′

Carcinoembryonic antigen hairpin oligonucleotide (CEA-HO): 5′-Biotin-CCA CGA TAC CAG CTT ATT CAA TTC GTG G-(CH2)6-SH-3′

Carcinoembryonic antigen single-stranded DNA (CEA-ssDNA): 5′-A TAC CAG CTT ATT CAA TTC GTG G-SH-3′

Carcinoembryonic antigen test DNA (CEA-tDNA): 5′-Biotin-CCA CGA TAC CAG CTT ATT CAA T-3′

Carcinoembryonic antigen control DNA (CEA-cDNA): 5′-Biotin-CCA CGA ATT GAA TAA GCT GGT ATC GTG G-3′

All chemicals used in this study were purchased from standard commercial sources and all were analytical reagent grade. All buffer solutions were prepared with ultra-pure (18.2 M $cm^{-1}$) water from a Millipore Milli-Q water purification system (Billerica, MA).

### 2.2. Preparation of condensed gold nanoparticles (AuNPs) and HO

AuNPs with different average diameter were prepared using the citrate reduction method according to the reported (He et al., 2012). All glasswares used in this study were thoroughly cleaned in aqua regia (three parts HCl and one part $HNO_3$), rinsed in doubly distilled water, and oven dried prior to use. Different volumes of 1% trisodium citrate was put in a 250 mL, round-bottom flask, containing 100 mL of 0.01% boiled $HAuCl_4$ aqueous solution. After the color of the solution changed, boiling was pursued for an additional 10 min; then the colloid solution was stirred for another 15 min without heating any more. The resulting AuNPs solution was stored in amber laboratory bottles at 4 °C and characterized by TEM and UV. We condensed the AuNPs by centrifugation for 15 min at 12,000 rpm. After discarding the supernatant, the remanent red pellets were collected at 4 °C. Finally, the AuNPs with average diameter 15 nm $\pm$ 3.5 nm were chosen to be condensed as 5-fold AuNPs solution to prepare the HO-AuNPs-ssDNA receptors.

Hairpin oligonucleotide (HO) was modified with a biotin at its 5′ end and a thiol at its 3′ end. It experienced a centrifugal 10 min under 1200 rpm first, then dispersed in the buffer (Tris–HCl (20 mM, pH 7.4), 100 mM NaCl, and 5 mM $MgCl_2 \cdot 6H_2O$). The solution was incubated in 95 °C water for 5 min and then allowed to slowly cool to room temperature (RT) over another 30 min so that the probe HO correctly folded into a hairpin structure. Tris(2-carboxyethyl) phosphine (TCEP), a thiol deoxidizer, was used to cut the disulfide bond formed between the thiol groups. And deoxyadenosine triphosphate (DATP), a monomer unit of nucleic acid, was used as sealant to prepare the HO-AuNPs conjugates (Huang et al., 2014).

### 2.3. Preparation of HO-AuNPs-ssDNA conjugates

Different molar ratios of the slight modified HO and thiolated single-stranded DNA (3/1, 2/1, 1/1, 1/2, and 1/3) (Qin et al., 2015a,b) and 15 μL of 1 mM TCEP were added into 1 mL of the 5-fold concentrated AuNPs solution to prepare HO-AuNPs-ssDNA conjugates, respectively. After shaking 2 h at RT, 90 μL of 15 mM DATP were attached to the solution and shook another 1 h at RT. Then, the HO-AuNPs-ssDNA conjugates were put at 4 °C for 6 h to increase the stability of the conjugates. The excess reagents were removed by centrifugation for 15 min at 12,000 rpm. After discarding the supernatant, the red pellets were washed twice with an aqueous solution containing 20 mM $Na_3PO_4 \cdot 12H_2O$, 5% BSA, 0.25% Tween-20, and 10% sucrose, through the centrifugation time of 10 min at 12,000 rpm; finally, redispersed in 1 mL the same buffer solution and stored at 4 °C before further use. All receptors (a–f) were synthesized in this way.

### 2.4. Preparation of streptavidin-biotinylated test/control DNA (SA-tDNA/SA-cDNA) conjugates

The streptavidin-biotinylated test/control DNA (SA-tDNA/SA-cDNA) conjugates were obtained using the previously reported method (Ge et al., 2013; Fang et al., 2014). Briefly, five hundred microlitre of 4 mg/ml of streptavidin was mixed with 10 μM biotinylated test/control DNA. The mixture was incubated for 2 h at room temperature. After adding 400 μL PBS (pH=7, 0.01 M) into the mixture, the solution was centrifuged in dialysis tube for 10 min at 12,000 rpm under RT, then discarded the supernatant. The above step was repeated for three times. The remaining solution in filter was diluted to 600 μL with PBS.

### 2.5. Preparation of the lateral flow biosensor (LFB)

The biosensor consists of three components: sample pad,

nitrocellulose (NC) membrane, and absorbent pad. The polyester fiber (PR-VL78) was applied to prepare the sample pad (23 mm × 30 cm) before it was immersed in the sample pad buffer (pH8.0) containing (0.25% TritonX-100, 0.02 M Tris–HCl, and 0.15 M NaCl) for 1 h, then dried at 37 °C for 2 h and at last stored in desiccators at RT before use. SA was utilized to combine with the biotinylated test/control DNA to form the (SA-tDNA/SA-cDNA) conjugates, so that the test-2 and control probes could be immobilized on the NC membrane. So, the test zone and control zone would not be easily washed away by the sample solution if probes are directly dispensed on the NC membrane. The test zone and control zone on the NC membrane (25 mm × 30 cm) were prepared by dispensing a concentration of 2 mg/mL SA, 2 mg/mL SA-tDNA and 2 mg/mL SA-cDNA solutions, respectively, with the HM3030 dispenser (Shanghai Kinbio Tech. Co., Ltd. Shanghai, China). The distance between three zones was around 0.5 cm. The membrane was dried at RT for 1 h and stored at 4 °C. Finally, all of the parts were assembled on a plastic adhesive backing layer (60 mm × 30 cm). The sample pad and absorbent pad were fabricated with 2 mm overlapped to ensure the solution migrating through the biosensor during the assay. Strips with a 4.0 mm width were cut by using the programmable strip cutter CTD300P and put in sample bags at 4 °C before use.

### 2.6. Analytical procedure of detect proteins using the strip biosensors array

In our test, HO-AuNPs-ssDNA conjugates and different

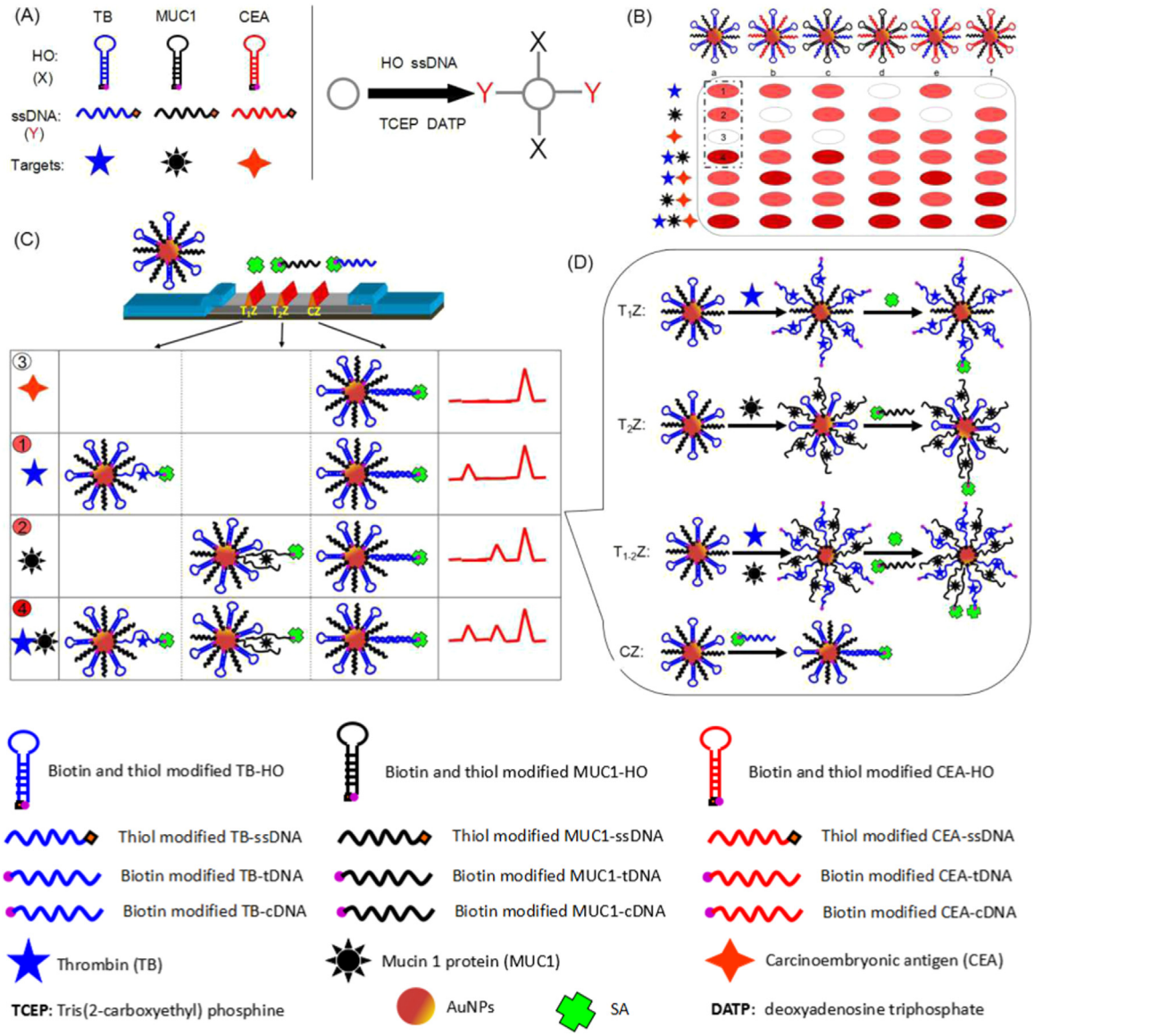


**Scheme 1.** (A) Design principles of self-assembled protein receptors based on aptamer-modified AuNPs. (Left) All types of aptamer components, (right) synthesis of protein receptors. (B) Schematic representation of the lateral flow array with selectivity toward a biomarker group (thrombin (TB), mucin 1 protein (MUC1) and carcinoembryonic antigen (CEA), which interact with their corresponding aptamers in the receptors a–f of the array). (C) Illustration of the configuration of the conventional strip biosensor and the interaction of receptor-a (TB-HO-AuNPs-MUC1-ssDNA) with two different proteins (TB, MUC1). The test-1 zone (T1Z): 2 mg/mL streptavidin (SA), the test-2 zone (T2Z): 2 mg/mL streptavidin-biotinylated mucin 1 protein test DNA (MUC1-SA-tDNA), the control zone (CZ): 2 mg/mL streptavidin-biotinylated thrombin control DNA (TB-SA-cDNA). The sample solutions are incubated for 12 h before dispensed to the sample pad. (D) Detailed description of the target-aptamer recognition reaction on different sites. On the T1Z: a folded thrombin hairpin oligonucleotide (TB-HO) transforms to an unfolded structure due to the target TB-inducer, the exposed activated-biotins (modified on TB-HO) are captured by the preimmobilized SA. On the T2Z: MUC1 firstly recognizes mucin 1 protein single-stranded DNA (MUC1-ssDNA) during the preincubation time and then migrates to be catched by streptavidin-biotinylated mucin 1 protein test DNA (MUC1-SA-tDNA), forming a MUC1-ssDNA/MUC1/MUC1-SA-tDNA sandwich format. However, Hybridization reaction (base-pairing interactions:A–T, C–G) is achieved on the CZ.

concentrations of proteins were agitated vigorously with a pipette for a little while and then incubated at room temperature for 12 h. 60 μL mixed solution was applied to the each biosensor, then the biosensor was washed by adding 30 μL of running buffer (1% PBSB). After reaction for 10 min at room temperature, the solution was applied to the sample application well and the test zone and control zone were evaluated visually. Qualitative detection (for high concentration of targets) can be realized by observing the color of test zone with the naked eyes. For quantitative measurements, the optical intensity of the red band was recorded using the portable "strip reader" instrument combined with "GoldBio strip reader" software.

For detection of proteins in real human plasma, the sample solutions were prepared by spiking different quantities of standard target solution into the plasma. The addition of plasma would lead to the matrix effect, so the volume of plasma was optimized before the experiment. Different volumes of plasma spiked with target was added to the sample application pad, and then the biosensor was washed with running buffer. The signal was recorded with the strip reader after 10 min. A better performance in terms of higher signal-to-noise ratio was obtained when the primary plasma liquid was diluted 50 times. Diluted human plasma spiked with different quantities of proteins was applied onto the strip biosensor array, and other steps were same as above said.

## 3. Results and discussion

### 3.1. Design principle of the strip biosensors array

The aptamers functionalized with gold nanoparticles (AuNPs) as receptors (a–f) that composed of corresponding hairpin oligonucleotide (HO) and their single-stranded DNA (ssDNA) (Scheme 1A (left)) have a variety of specific identification. They could be rapidly synthesized using a mixed self-assembled strategy (Scheme 1A, right). In forming the protein-detecting array, the "one-pot" reaction of 5-fold AuNPs solution, tris (2-carboxyethyl) phosphine (TCEP), an excess of two different structure oligonucleotides chosen from a pool and deoxyadenosine triphosphate (DATP) led to a mixture of six different products (protein receptors a–f, Scheme 1B) (Chen et al., 2014; Huang et al., 2014; Chen et al., 2013). In our study on protein (Scheme 1C), 2 mg/mL streptavidin (SA), 2 mg/mL streptavidin-biotinylated test DNA (SA-tDNA) and 2 mg/mL streptavidin-biotinylated control DNA (SA-cDNA) solutions were preimmobilized on the NC membrane to form the test-1 zone (T1Z), test-2 zone (T2Z) and the control zone (CZ). The sample solutions containing TB, MUC1 and TB-HO-AuNPs-MUC1-ssDNA conjugates went through a 12 h preincubation step before applied to the LFB sample pad. The complexes migrates via capillary action, as recognition reactions, protein detection on the T1Z was realized by target TB-induced a conformational transition of thrombin hairpin oligonucleotide (TB-HO) from an unfolded to a folded structure because it adopts a compact unimolecular quadruplex structure with two G-quartets, the exposed activated-biotins (modified on TB-HO) are captured by the preimmobilized SA on the T1Z to form the first characteristic red band because of the accumulation of AuNPs. The excess complexes continue to migrate to the T2Z and MUC1 recognized both mucin 1 protein single-stranded DNA (MUC1-ssDNA) and streptavidin-biotinylated mucin 1 protein test DNA (MUC1-SA-tDNA) to form a MUC1-ssDNA/MUC1/MUC1-SA-tDNA sandwich type. The AuNPs accumulated to produce the second characteristic red band. At last, hybridization reaction (base-pairing interactions:A–T, C–G) between TB-HO and TB-SA-cDNA was achieved on the CZ (Scheme 1D). We found that the aptamer gave a different response to target protein due to the various levels of the aggregation of AuNPs and caused a obvious color change on different sites (Scheme 1C). The color change was caused by different aggregation behaviors and could be observed by the naked eyes and a portable strip reader.

### 3.2. Detectability and anti-interference capability

One of the advantages of using aptamers for scaffolding these receptors is the simplicity by which a set of water-soluble, multifunctional protein receptors can be obtained by self-assembly. To determine whether this array functions properly and has an obvious color change, we detected different target proteins and other interfering proteins. As shown in Fig. S1A, for receptor-b, in the absence of the targets, there is only one red band on the CZ. When 100 nM thrombin (TB) was added, TB induced conformational changes of thrombin hairpin oligonucleotide (TB-HO), the exposed activated biotins were captured by the preimmobilized streptavidin (SA) on the T1Z to form the first characteristic red band. When 100 nM carcinoembryonic antigen (CEA) was added, CEA recognized both CEA single-stranded DNA (CEA-ssDNA) and streptavidin-biotinylated CEA test DNA (CEA-SA-tDNA) to form a CEA-ssDNA/CEA/CEA-SA-tDNA sandwich type, which produced the second red band. However, when 100 nM mixed TB-CEA was added, two different reactions could occur one after another and ultimately generate two red bands in different locations. Their corresponding optical intensities in Fig. S1B supported the phenomena. To confirm the manifestation of the "self assembly", which should endow the modified aptamers with selectivity toward proteins, we performed two complementary experiments. In the first, we incubated the different receptors (a–f) with various proteins and compared their optical intensities (Fig. S2A). In the second experiment, the different receptors were treated with common serum proteins (Fig. S2B). Remarkably, whereas receptors a–f exhibited a strong response to nanomolar concentrations of proteins, only a small or negligible effect was observed for the control sensor. These results show that the optical intensities in our system mainly originate from the interaction of the receptors with proteins.

### 3.3. Optimization of experimental parameters

To obtain better sensitivity, specificity, selectivity, reproducibility and detectability for the detection of proteins, the experimental parameters were systematically optimized. The varied sizes of AuNPs are synthesized using the citrate reduction method (Chen et al., 2014; Huang et al., 2014; Chen et al., 2013). The faster the capping of AuNPs by the citrate, the smaller the resulting nanoparticles (Fig. 1A). The optical intensities of the receptor-b upon addition of proteins peaked at the size of 16 nm (Fig. 1B). The color changed from nacarat to violet (Fig. 1C) and the surface plasma absorption maximum changed from 518 nm to 540 nm (Fig. S3) depending on the sizes (Table S1). Take all factors into account, we chose the AuNPs with average diameter 15 nm $\pm$ 3.5 nm as the ideal nanoparticles.

The molar ratio of hairpin oligonucleotide (HO) to single-stranded DNA (ssDNA) could influence the forming of the receptors. High level of mixed chimerism led to high yield of AuNP aggregates, whereas the low proportion led to inadequate streptavidin capture. Different molar ratios from HO to ssDNA were used to mix. As is shown in Fig. S4A, the peak areas on the TZ and the S/N ratios show consistency; both increased with decreasing molar ratios from 3/1 to 1/1 and then decreased from 1/1 to 1/3. So, we selected 1/1 as the best ratio.

The volume of DATP is crucial in the sensing system because it is a commonly used stabilized additive to preserve the aptamer activity and connections. Five varying volume of DATP were tested (Fig. S4B), their optical intensities and *S*/*N* ratios were altered as

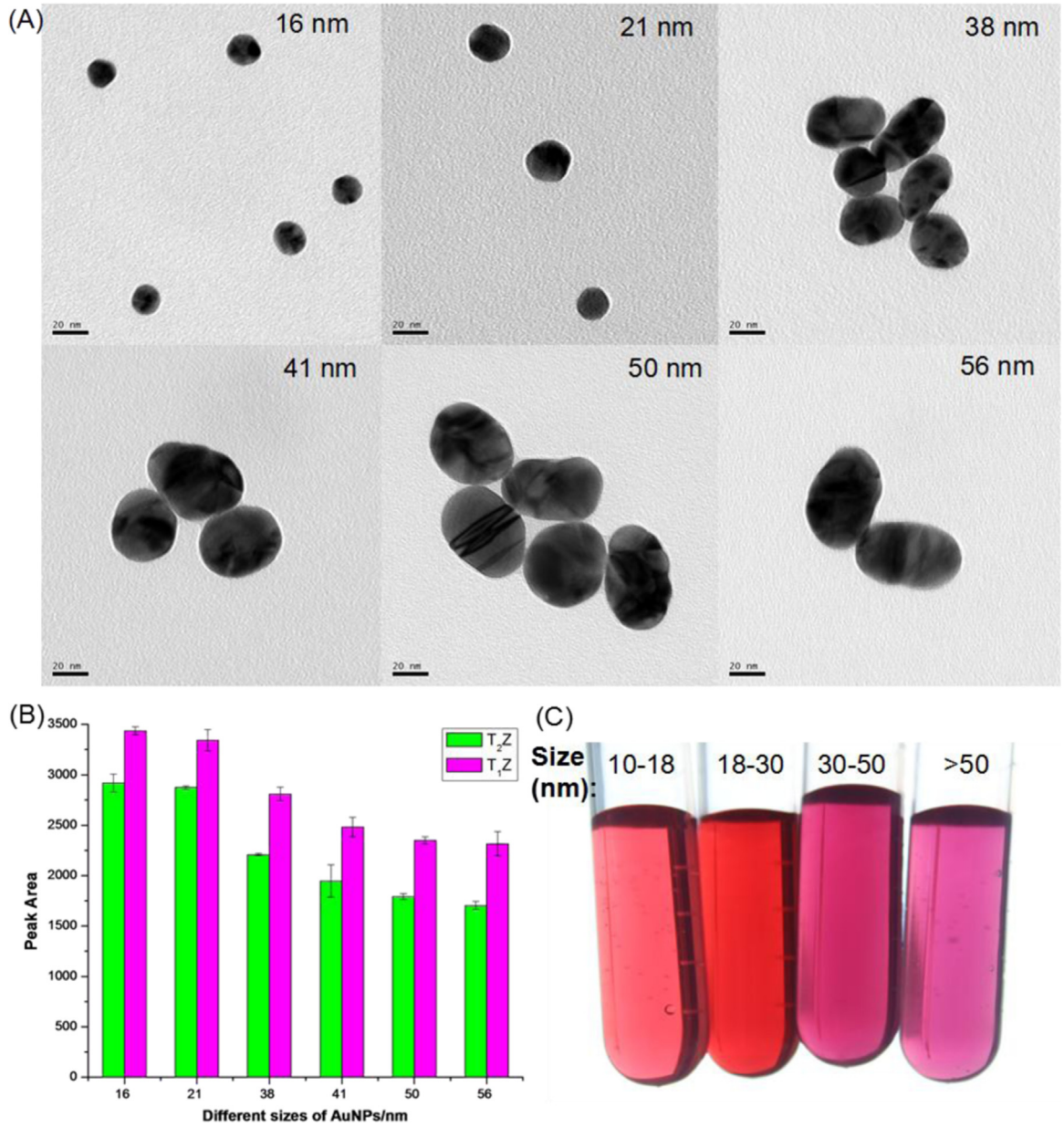


**Fig. 1.** (A) Transmission electron microscopy (TEM) images of the different sizes of AuNPs: all scale bars=20 nm, the sizes of AuNPs are 16 nm, 21 nm, 38 nm, 41 nm, 50 nm and 56 nm, respectively. (B) Corresponding optical intensities of the receptor-b upon addition of 100 nM proteins. (C) Photographs of aqueous solutions of gold nanospheres.

the volumes of DATP changed, and they reached a maximum when it was 30 μL.

The reaction time (Fig. S4C) between the intermediate product and DATP is a significant factor that can adversely affect the stability of the final product. The peak areas and the *S*/*N* increased with increasing reaction time and then reached a maximum when the reaction time was 2 h, indicating that a thorough reaction had occurred and the self-assembly process had completed.

For the effective self-assembly of the LFB and the high sensitive to the target, we have studied the differences about the stored methods of the resulting conjugate solution. The conjugates were stored at 4 °C or in glass fiber. As shown in the Fig. S5, we find that the detectabilities of these two methods are almost the same, but the standard deviations of three independent measurements are different. We chose the more accurate one, that is the 4 °C storage of conjugates.

We have also evaluated the effect of the concentration of streptavidin (SA) immobilized on the test/control zone on the response of the logic system. We have studied the effect of (A) 0.5 mg/mL (B) 1 mg/mL (C) 2 mg/mL and (D) 4 mg/mL SA on the test zone and control zone for receptor-b on the responses of 100 nM targets in "OR" logic gate in the Fig. S6. We find that the concentration of SA immobilized on the test/control zone did not change the phenomenon of the logic states, but influence the intensities of the signals. The 2 mg/mL SA is the ideal concentration.

Further taking the saturability of LFB, the consumption of reagent and the cost per assay into consideration, we chose the 5-fold AuNPs with average diameter 15 nm ± 3.5 nm, 1/1 of HO to ssDNA, 30 μL DATP, 2 h reaction time, the 4 °C storage of conjugates and 2 mg/mL SA as the optimized parameters throughout the experiments.

### 3.4. Molecular logic gate

Molecular logic gates controlled by DNA oligonucleotide inputs are most well-developed DNA logic constructs. The system quite

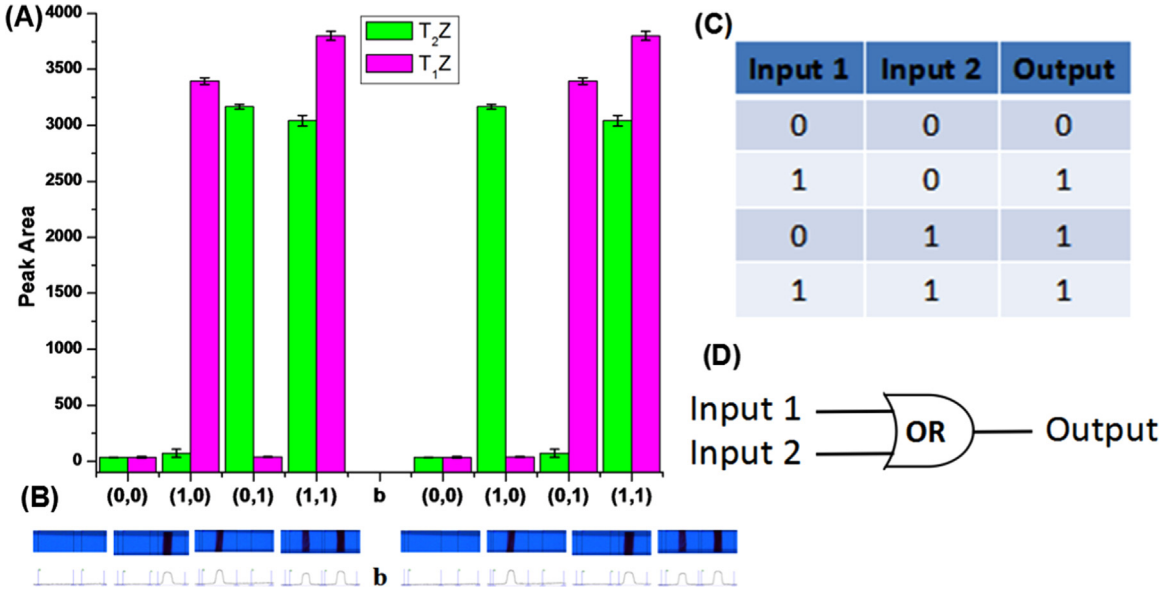


**Fig. 2.** "OR" gate. (A) Normalized optical intensities (peak areas of the red bands on the TZ). (B) Typical photo images and recorded responses of the red bands on the TZ and CZ. (C) Truth table and (D) logic scheme of the "OR" logic gate with different combinations upon targets at 100 nM. (For interpretation of the references to color in this figure legend, the reader is referred to the web version of this article.)

differently responds in the absence of protein molecules due to the thermal instability of target-free aptamer complex. The mode of operation of the "OR" logic circuit is illustrated in Scheme S1. For every receptor, two targets proteins are as the two inputs, The inputs are considered as "1" when they are present and "0" if they are absent. The color and the optical intensities of the TZ are regarded as the output, with the absence and presence of red bands on the TZ defined as "0" and "1", separately. No red band was observed on the TZ only for the (0,0) input state, however significant red bands were observed for other input combinations. The corresponding optical intensities are shown in Fig. 2A–B. Accordingly, the system state (0,1), (1,0), (1,1) yielded high peak areas. The biocomputing responses obtained from the DNA circuit correspond to the truth table expected for the sequence of the "OR" logic gate (Fig. 2C–D). And a set of two-input logic gates were constructed via similar strategies, such as "AND" (Scheme S2 and Fig. S7), "OR" (Fig. S8), "INH" (Scheme S3 and Fig. S9) and "NAND" (Fig. S10) logic gates. We also find that when we varied the order of the two input signals in two different permutations (target-1, target-2) or (target-2, target-1), there will be 12 permutations in our array. If we set one state was a correct password, which means the lock will be opened and cannot be closed again. Then all other wrong states cannot open the lock. So, We have reason to believe that it has the potential application in the keypad-lock security system (Chen et al., 2012, 2013).

Based on both this conjecture and the principle of the two-input gates, other-input were designed, such as three-input: "AND–OR" (Fig. S11), "AND–INH" (Fig. S12), "OR–INH" (Fig. S13), "INH–NAND" (Fig. S14); four-input: "AND–OR–INH" (Fig. S15), "AND–INH–NAND" (Fig. S16), "OR–INH–NAND" (Fig. S17) as well as five-input: "AND–OR–INH–NAND" (Figs. 3 and S18–S22). The ability to integrate molecular components remains crucial for the construction of more-complicated molecular devices. Herein, the versatility of the inputs permitted implementation of more-complex molecular logic circuits. The "AND–OR–INH–NAND" logic gate for receptor-b upon addition of different proteins was constructed in Fig. 3. Logic scheme (Fig. 3C) and truth table (Fig. 3D) told us the five inputs and the 32 system states. This combinated gate produces an output of "1" only in these states: (11000), (10100), (11100), (11010), (10110), (11110), (11001), (10101), (11101), (11011), (10111) and (11111), while an output of "0" was produced in other states. The results supported the conclusion (Fig. 3A–B). When we varied the order of the five input, there will be 64 permutations in our strip biosensors array. It means that the present system based on aptamers modified AuNPs may eventually be applicable to the keypad-lock system with enhanced complexity one day (Chen et al., 2015).

### 3.5. Selectivity and practicality

To demonstrate the selectivity and practicality of the protein sensor array prototype, we used receptors a–f to discriminate different proteins in two different environments (PBS, PH 7.4, Fig. 4A; real human plasma, Fig. 4B). Linear discriminate analysis (LDA), a statistic method for recognizing the linear combination of features that differentiate two or more classes of object, was used to differentiate quantitatively the response pattern of target proteins (Lu et al., 2013; Anzenbacher et al., 2010). Three canonical factors were generated (93.60%, 4.08%, and 2.32%) that represent linear combinations of the response matrices obtained from the response patterns (six aptamers × three proteins × four replicates). The 36 training cases were separated into three respective groups, with 100% accuracy according to the classification matrix derived from the analysis of subsets of the data sets, and the two factors that were most significant are plotted in Fig. 4A. In real human plasma, the 36 training cases were also separated into three respective groups with 100% accuracy. The three canonical factors are 84.46%, 14.69% and 0.85%, and the plot of the first two factors is presented in Fig. 4B. Analyzing the patterns using LDA resulted in markedly distinct clusters, which confirm the ability of the system to discriminate among different protein biomarkers in complicated biological mixtures.

### 3.6. Analytical performance

Under the optimum condition, the proposed strip biosensors array was utilized to test a series of sample solution with various concentrations. As is shown in Fig. S23, the color and recorded responses of the red bands on the T1Z and T2Z obviously deepened with the increasing concentration of targets. As a result, the

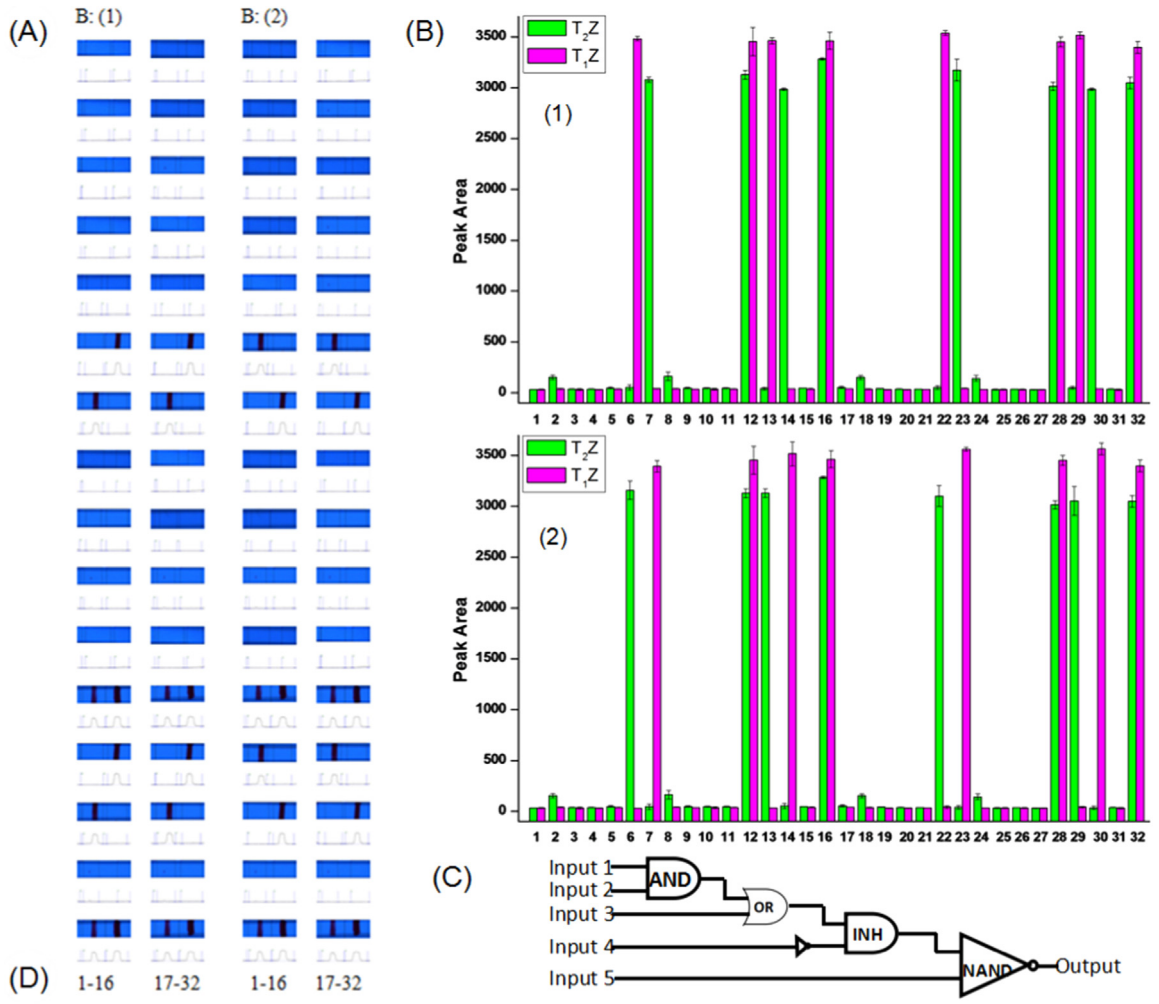


| Number | 1 | 2 | 3 | 4 | 5 | 6 | 7 | 8 | 9 | 10 | 11 | 12 | 13 | 14 | 15 | 16 | 17 | 18 | 19 | 20 | 21 | 22 | 23 | 24 | 25 | 26 | 27 | 28 | 29 | 30 | 31 | 32 |
|---|---|---|---|---|---|---|---|---|---|---|---|---|---|---|---|---|---|---|---|---|---|---|---|---|---|---|---|---|---|---|---|---|
| Input 1 | 0 | 1 | 0 | 0 | 0 | 1 | 1 | 1 | 0 | 0 | 0 | 1 | 1 | 1 | 0 | 1 | 0 | 1 | 0 | 0 | 0 | 1 | 1 | 1 | 0 | 0 | 0 | 1 | 1 | 1 | 0 | 1 |
| Input 2 | 0 | 0 | 1 | 0 | 0 | 1 | 0 | 0 | 1 | 1 | 0 | 1 | 1 | 0 | 1 | 1 | 0 | 0 | 1 | 0 | 0 | 1 | 0 | 0 | 1 | 1 | 0 | 1 | 1 | 0 | 1 | 1 |
| Input 3 | 0 | 0 | 0 | 1 | 0 | 0 | 1 | 0 | 1 | 0 | 1 | 1 | 0 | 1 | 1 | 1 | 0 | 0 | 0 | 1 | 0 | 0 | 1 | 0 | 1 | 0 | 1 | 1 | 0 | 1 | 1 | 1 |
| Input 4 | 0 | 0 | 0 | 0 | 1 | 0 | 0 | 1 | 0 | 1 | 1 | 0 | 1 | 1 | 1 | 1 | 0 | 0 | 0 | 0 | 1 | 0 | 0 | 1 | 0 | 1 | 1 | 0 | 1 | 1 | 1 | 1 |
| Input 5 | 0 | 0 | 0 | 0 | 0 | 0 | 0 | 0 | 0 | 0 | 0 | 0 | 0 | 0 | 0 | 0 | 1 | 1 | 1 | 1 | 1 | 1 | 1 | 1 | 1 | 1 | 1 | 1 | 1 | 1 | 1 | 1 |
| Output | 0 | 0 | 0 | 0 | 0 | 1 | 1 | 0 | 0 | 0 | 0 | 1 | 1 | 1 | 0 | 1 | 0 | 0 | 0 | 0 | 0 | 1 | 1 | 0 | 0 | 0 | 0 | 1 | 1 | 1 | 0 | 1 |

**Fig. 3.** "AND–OR–INH–NAND" logic gate. (A) Typical photo images, responses of the red bands on the TZ and CZ. (B) Optical intensities (peak areas of the red bands on the TZ). (C) Logic scheme and (D) truth table of the receptor-b upon addition of different proteins for the "AND–OR–INH–NAND" logic gate. (For interpretation of the references to color in this figure legend, the reader is referred to the web version of this article.)

optical intensities increased linearly with the logarithm of targets concentration, amazing linear equations and their correlation coefficients were explicitly as shown in Fig. 5. Their linear range and detection limit were clearly listed in the Table S2. Taken together, each receptor can detect two proteins, every aptamer can discern its homologous protein. Reactions independently occur on their respective areas and do not influence each other. For one protein, its ability of identification its hairpin oligonucleotide (HO) is much more stronger than that of its pure single-strand DNA (ssDNA). The best detection limit of TB, MUC1 and CEA can get 1.61 nM (Linear range: 3.2–250 nM), 1.13 nM (Linear range: 1.6–400 nM) and 0.7 nM (Linear range: 0.8–300 nM), which were comparable or even better than the other reported method aptasensors for proteins detection (Qin et al., 2015a,b; Altintas et al., 2011; Baek et al., 2014; Cheng et al., 2009; Li et al., 2014; Tang et al., 2006; Wang et al., 2013; Xu et al., 2009; Zhu et al., 2010) (Table S3).

### 3.7. *Stability and reproducibility*

Long-term storage assay was carried out to test the reproducibility and stability of the strip biosensors array. The strips were stored in sample sacks under desiccated conditions at 4 °C and 100 nM mixed TB-CEA were measured three times at different weeks under the optimized condition. As is shown in Fig. S24, similar color intensities and optical responses could be obtained from the strip biosensors receptor-b after the same time. The corresponding RSD values were 2.76% and 4.68%, 0.05% and 0.44%, 1.33% and 1.63%, 3.06 and 1.18%, respectively, indicating excellent analytical stability and reproducibility.

## 4. Conclusions

In conclusion, we have successfully introduced an array of aptamer modified gold nanoparticles to visually and quantificationally detect protein biomarkers, and we also constructed various

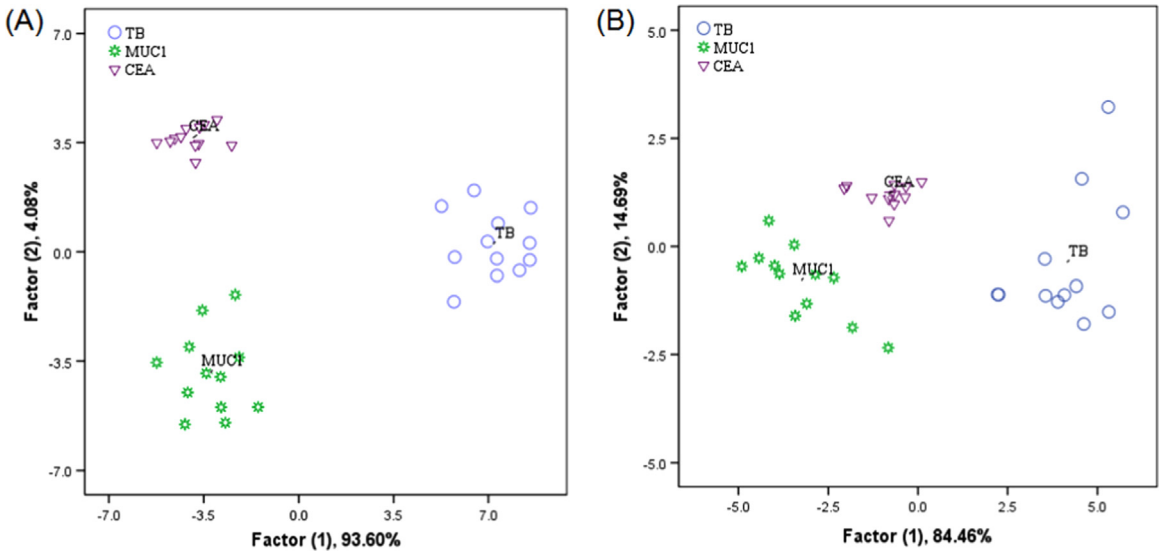


**Fig. 4.** Linear discriminate analysis (LDA) plot showing the response of the lateral flow array to different proteins at 100 nM in (A) PBS buffer (B) real human plasma samples.

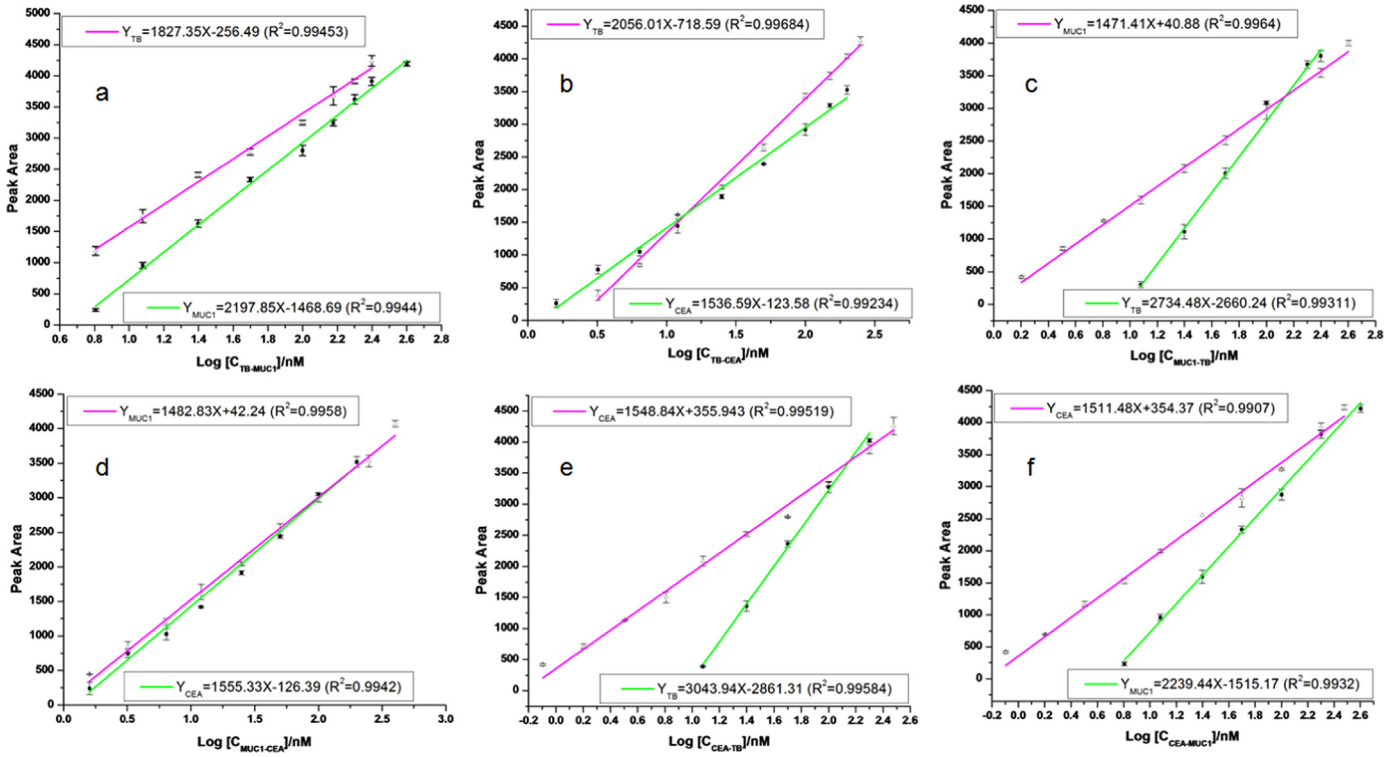


**Fig. 5.** Calibration curves show the linear relationships between the peak areas vs. the logarithm of different protein concentrations using the six receptors (a–f) in the array.

input logic circuits capable of operating as a biocomputing keypad-lock security system. In comparison with previously reports, the distinctive advantages of our proposed strip biosensors array are that: (1) it can be easily established owing to the design modularity and flexibility of aptamer and its classic aptamer-target sandwich recognition reactions; (2) it can simultaneously detect multiple proteins without mutual interference, accompanying with lower limit of detection and wider linear range; (3) by the use of the LFB, the results can be readily recognized by the naked eyes, which makes practical applications possible; (4) a complete set of four elementary logic gates (AND, OR, INH, and NAND) and eight combinative logic gates (AND–OR; AND–INH; OR–INH; INH–NAND; AND–OR–INH; AND–INH–NAND; OR–INH–NAND; AND–OR–INH–NAND) are realized using this array, which offers the potential application in the keypad-lock system with enhanced complexity.

## Acknowledgments

This work was supported by the National Natural Science Foundation of China (Nos. 21175032 and 21475032) and the Natural Science Fund for Creative Research Groups of Hubei Province of China (No. 2014CFA015).

## Appendix A. Supplementary material

Supplementary data associated with this article can be found in

the online version at http://dx.doi.org/10.1016/j.bios.2015.12.096.

## References


Angelos, S., Yang, Y.W., Khashab, N.M., Stoddart, J.F., Zink, J.I., 2009. J. Am. Chem. Soc. 131, 11344–11346.
Anzenbacher Jr., P., Lubal, P., Bucek, P., Palacios, M.A., Kozelkova, M.E., 2010. Chem. Soc. Rev. 39, 3954–3979.
Altintas, Z., Uludag, Y., Gurbuz, Y., Thothill, I.E., 2011. Talanta 86, 377.
Berezovski, M., 2005. J. Am. Chem. Soc. 127, 3165–3171.
Baek, S.H., Wark, W.W., Lee, H.J., 2014. Anal. Chem. 86, 9824–9829.
Cox, J.C., Ellington, A.D., 2001. Bioorg. Med. Chem. 9, 2525–2531.
Chen, J.H., Zhou, S.G., Wen, J.L., 2014. Anal. Chem. 86, 3108–3114.
Chen, J.H., Zhou, X.M., Zeng, L.W., 2013. Chem. Commun. 49, 984–986.
Chen, J.H., Fang, Z.Y., Lie, P.C., Zeng, L.W., 2012. Anal. Chem. 84, 6321–6325.
Chen, J.H., Zhou, S.G., Wen, J.L., 2015. Angew. Chem. Int. Ed. 54, 446–450.
Cheng, A.K.H., Su, H.P., Wang, A., Yu, H.Z., 2009. Anal. Chem. 81, 6130–6139.
Famulok, M., Mayer, G., 2011. Acc. Chem. Res. 44, 1349–1358.
Feng, L.Y., Lyu, Z.Z., Offenhausser, A., Mayer, D., 2015. Angew. Chem. Int. Ed. 54, 7693–7697.
Fang, Z.Y., Wu, W., Lu, X.W., Zeng, L.W., 2014. Biosens. Bioelectron. 56, 192–197.
Ge, C.C., Yu, L.X., Fang, Z.Y., Zeng, L.W., 2013. Anal. Chem. 85, 9343–9349.
He, Y.Q., Zhang, B., Man, F., Abdel, K., Liu, G.D., 2012. Biosens. Bioelectron. 34, 37–43.
Huang, Y., Wen, W., Du, D., Zhang, X.H., Wang, S.F., Lin, Y.H., 2014. Biosens. Bioelectron. 54, 578–584.
Janssen, B.M.G., Rosmalen, M. Van, Van Beek, L., Merkx, M., 2015. Angew. Chem. Int. Ed. 54, 2530–2533.
Liu, Z., Zhang, W., Hu, L., Li, H., Zhu, S., Xu, G., 2010. Chem. Eur. J. 16, 13356–13359.
Lin, Y.H., Xu, C., Ren, J.S., Qu, X.G., 2012. Angew. Chem. 124, 12747–12751.
Lu, Y.X., Liu, Y.Y., Zhang, S.G., Wang, S., Zhang, S.C., Zhang, X.R., 2013. Anal. Chem. 85, 6571–6574.
Li, L., Li, W.P., Ma, C., Yang, H.G., Ge, S.G., Yu, J.H., 2014. Sens. Actuators B 202, 314.
Pu, F., Ju, E.G., Ren, J.S., Qu, X.G., 2014. Adv. Mater. 26, 1111–1117.
Qin, C.Y., Wen, W., Zhang, X.H., Gu, H.S., Wang, S.F., 2015a. Chem. Commun. 51, 8273–8275.
Qin, C.Y., Wen, W., Zhang, X.H., Gu, H.S., Wang, S.F., 2015b. Analyst 140, 7710–7717.
Stojanovic, M.N., Stefanovic, D., Rudchenko, S., 2014. Acc. Chem. Res. 47, 1845–1853.
Seelig, G., Soloveichik, D., Zhang, D.Y., Winfree, E., 2006. Science 314, 1585–1588.
Silva, A.P.De, Uchiyama, S., 2007. Nat. Nanotechnol. 2, 399–410.
Tuerk, C., Gold, L., 1990. Science 249, 505–510.
Tang, D.Q., Zhang, D.J., Tang, D.Y., Ai, H., 2006. J. Immonogical Methods 316, 144.
Uchiyama, S., Kawai, N., Silva, A.P.De, Iwai, K., 2004. J. Am. Chem. Soc. 126, 3032–3033.
Wilson, D.S., Szostak, J.W., 1999. Annu. Rev. Biochem. 68, 611–647.
Wang, X., Zhou, M., Zhu, Y., Miao, J., Mao, C., Shen, J., 2013. J. Mater. Chem. B 1, 2132.
Xu, H., Mao, X., Wang, S.F., Kawde, A.N., Liu, G.D., 2009. Anal. Chem. 81, 669–675.
Zhu, Z., Wu, C.C., Liu, H.P., Yang, C.J., Tan, W.H., 2010. Angew. Chem. Int. Ed. 49, 1052.